Anticorrosive Assay-Guided Isolation of Active Phytoconstituents from *Anthemis pseudocotula* Extracts and a Detailed Study of Their Effects on the Corrosion of Mild Steel in Acidic Media

H. Z. Alkhathlan*, M. Khan, M. M. S. Abdullah, A. M. Al-Mayouf, A. Yacine Badjah-Hadj-Ahmed, Z. A. ALOthman, A. A. Mousa

Department of Chemistry, College of Science, King Saud University, P.O.Box 2455, Riyadh - 11451, Saudi Arabia.

*To whom correspondence should be addressed: *E-mail: khathlan@ksu.edu.sa*

Tel: +966-1-4675910, Fax: +966-1-4675992.

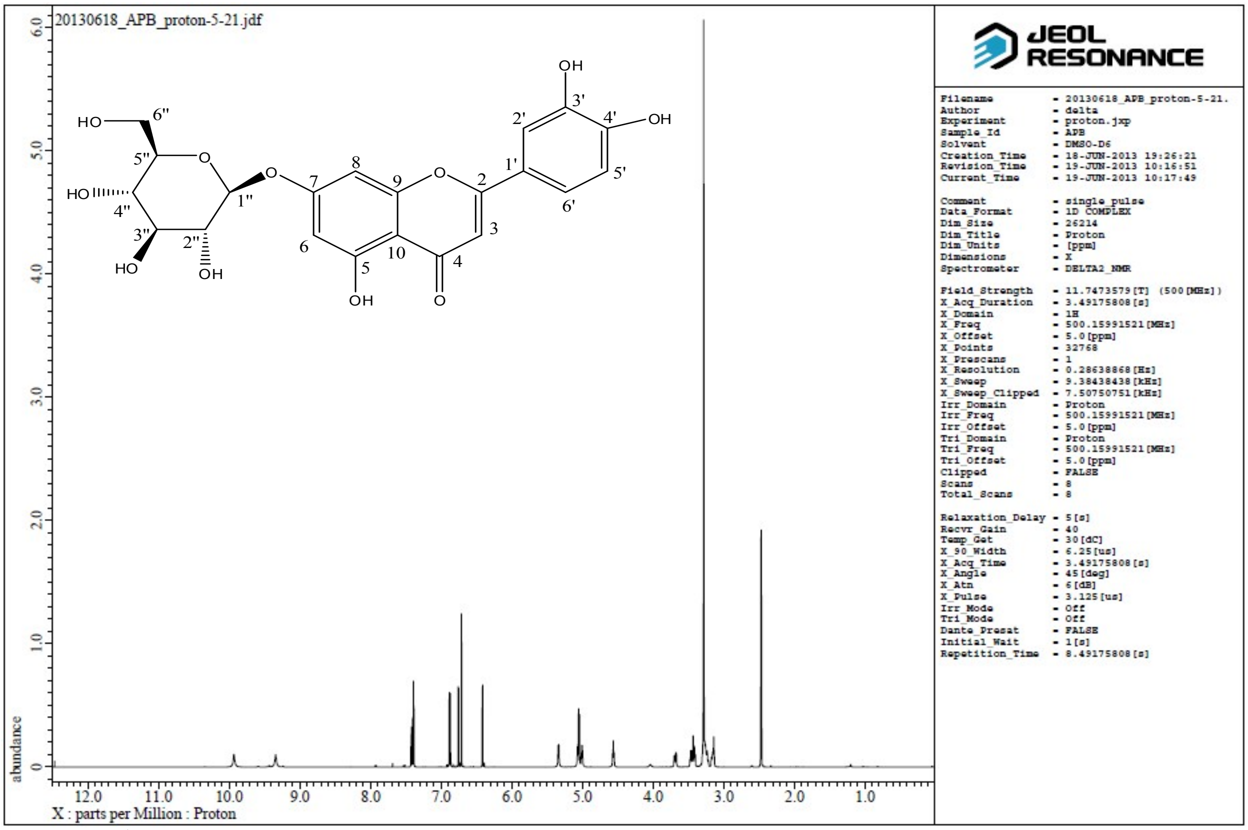

Fig. S1a. ^{1}H NMR spectrum of luteolin-7-O-β-D-glucoside (**APB**) in DMSO-d_6.

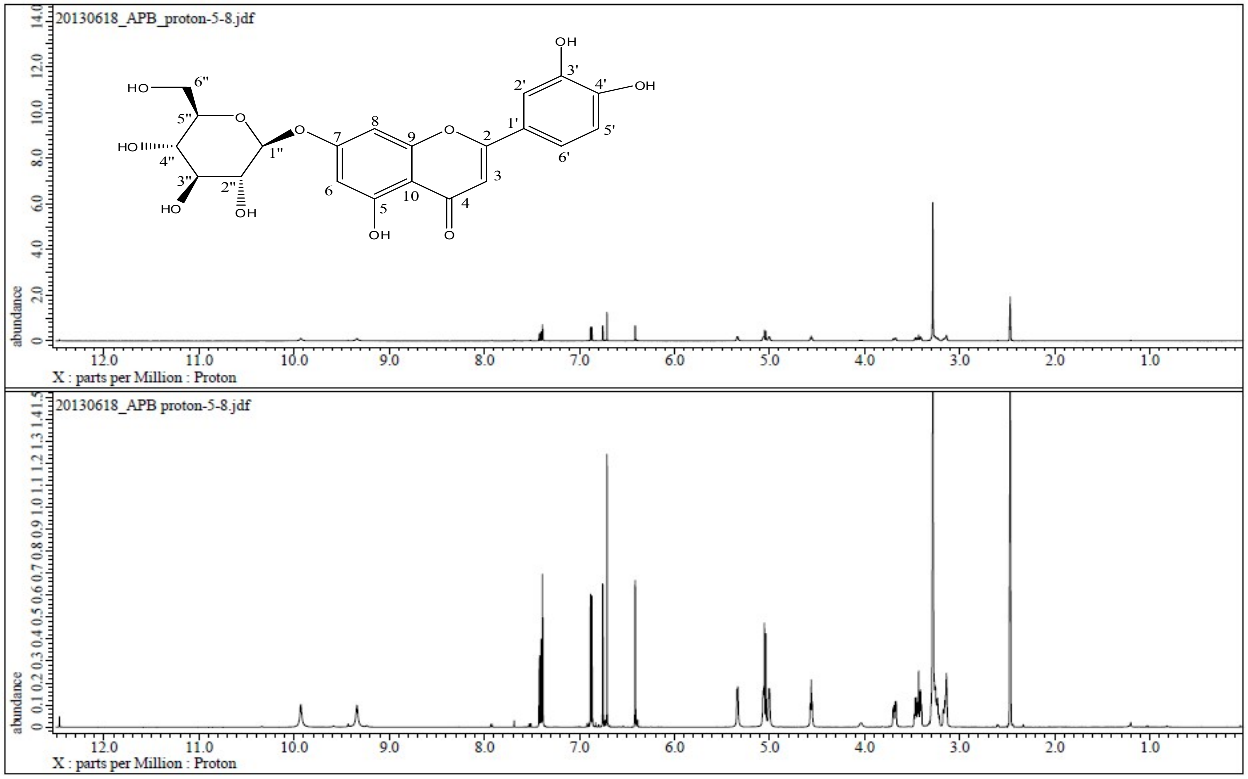

Fig. S1b. Expanded ^{1}H NMR spectrum of luteolin-7-O-β-D-glucoside (**APB**) in DMSO-d_6.

Fig. S1c. Expanded ^{1}H NMR spectrum of luteolin-7-O-β-D-glucoside (**APB**) in DMSO-d_6.

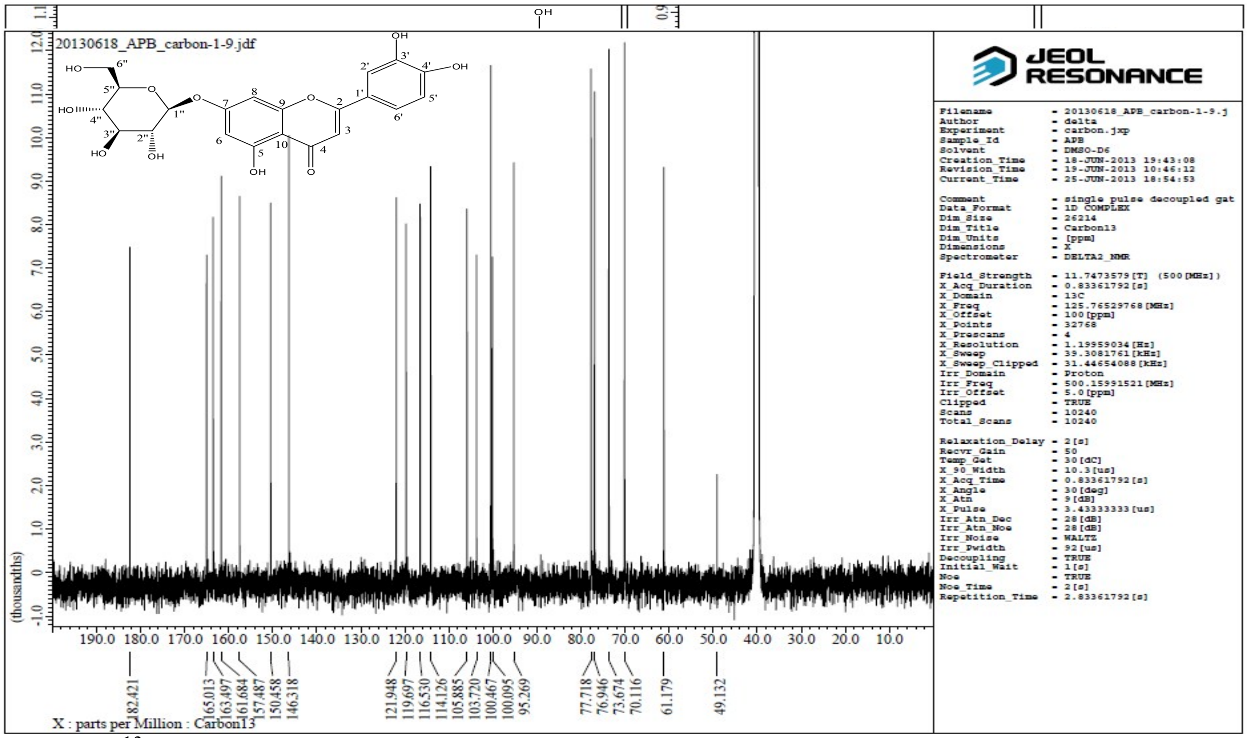

Fig. S2a. ^{13}C NMR spectrum of luteolin-7-O-β-D-glucoside (**APB**) in DMSO-d_6.

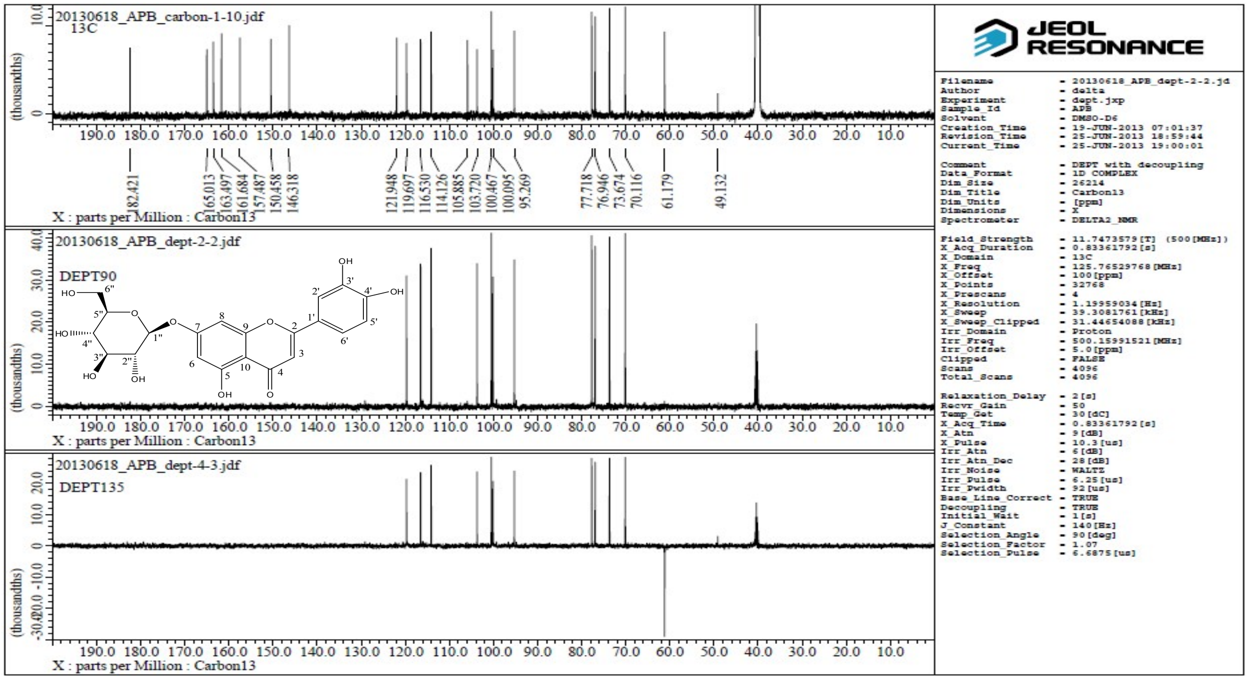

Fig. S2b. DEPT spectrum of luteolin-7-O-β-D-glucoside (**APB**) in DMSO-d_6.

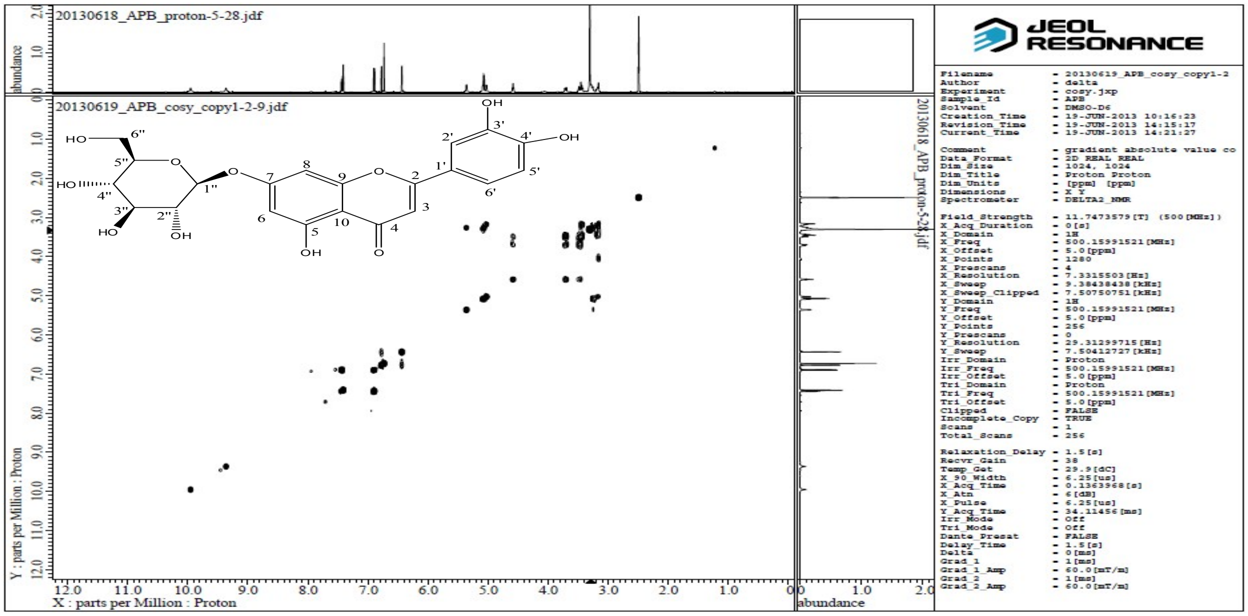

Fig. S3a. COSY spectrum of luteolin-7-O-β-D-glucoside (**APB**) in DMSO-d_6.

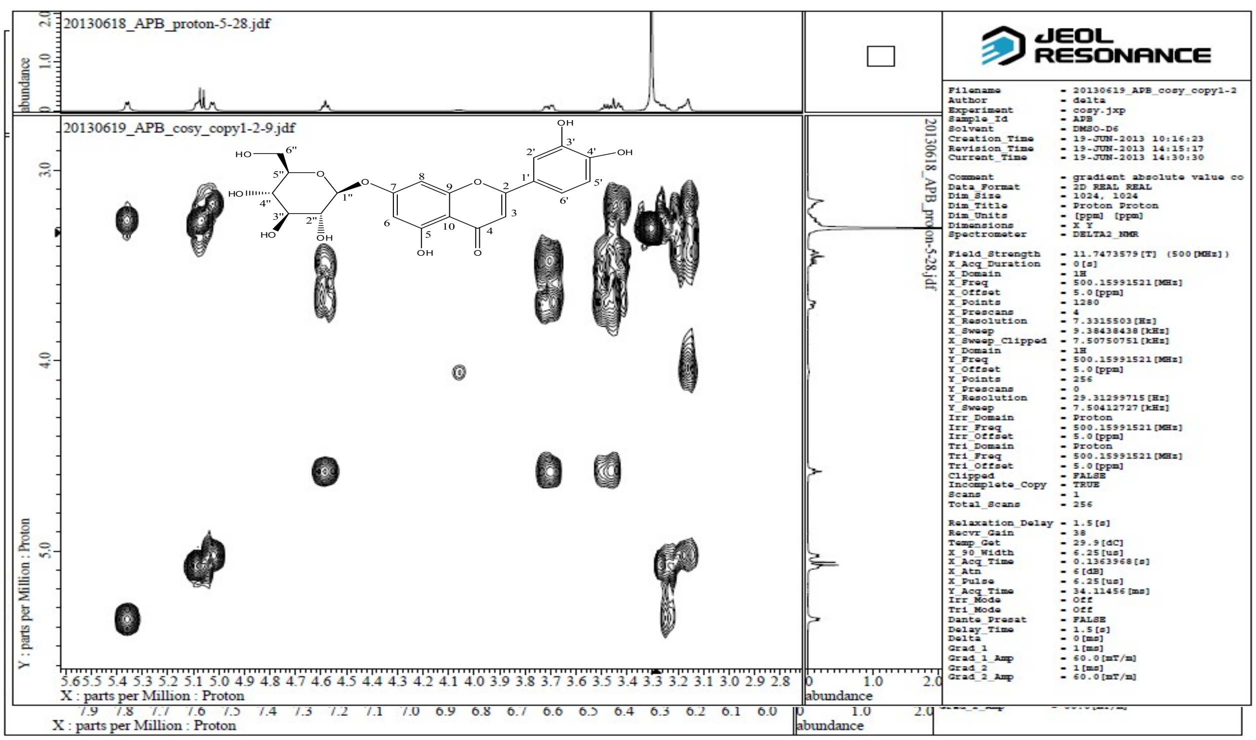

Fig. S3b. Expanded COSY spectrum of luteolin-7-O-β-D-glucoside (**APB**) in DMSO-d_6.

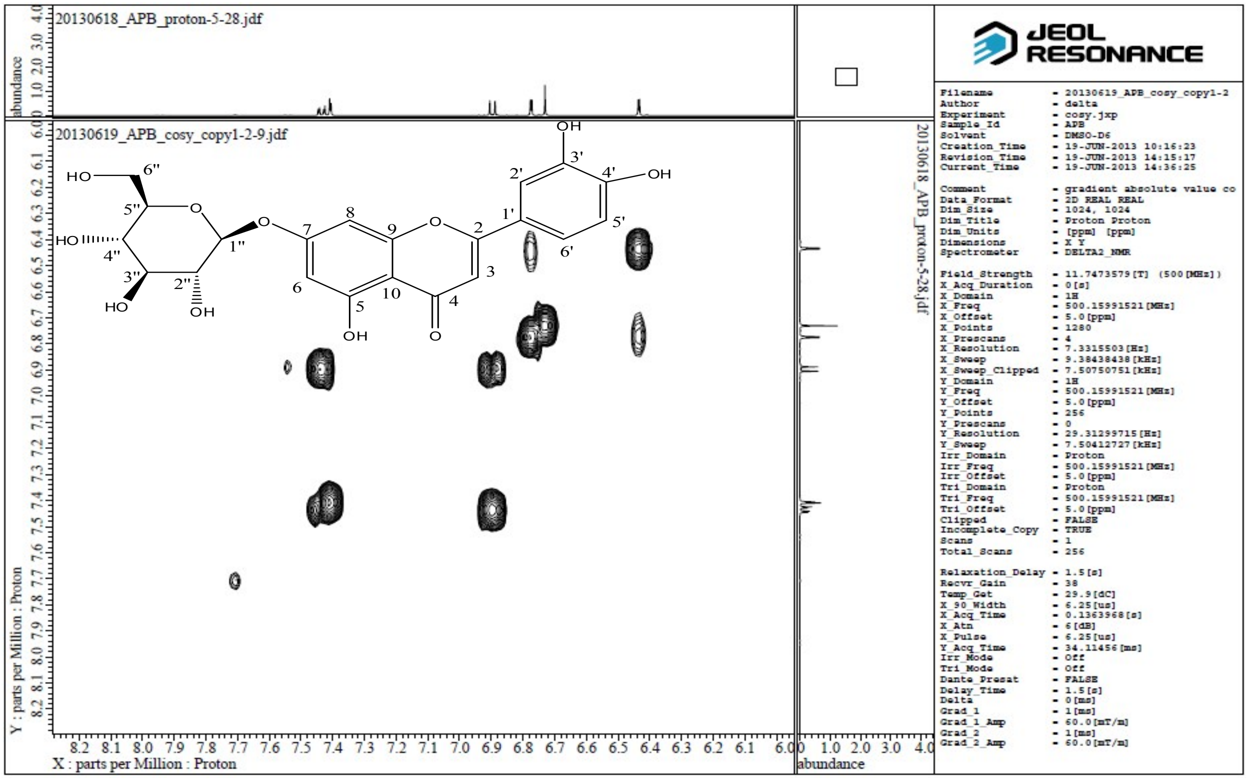

Fig. S3c. Expanded COSY spectrum of luteolin-7-O-β-D-glucoside (**APB**) in DMSO-d_6.

Fig. S4a. HMQC spectrum of luteolin-7-O-β-D-glucoside (**APB**) in DMSO-d_6.

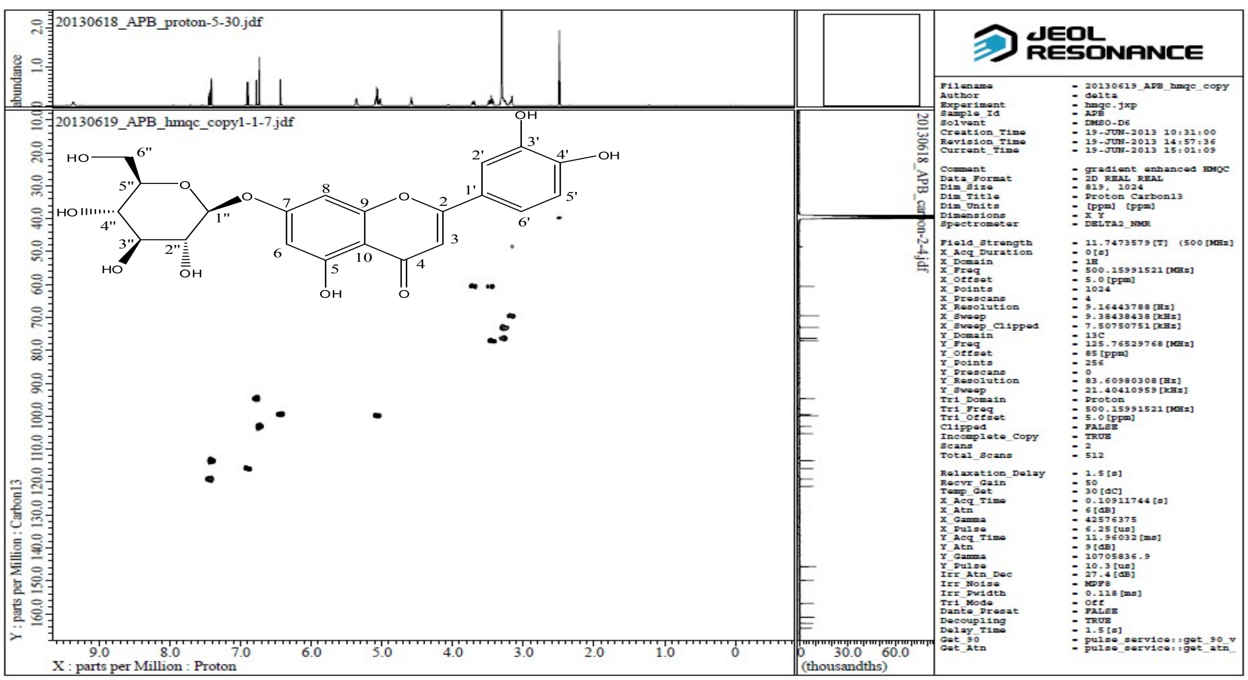

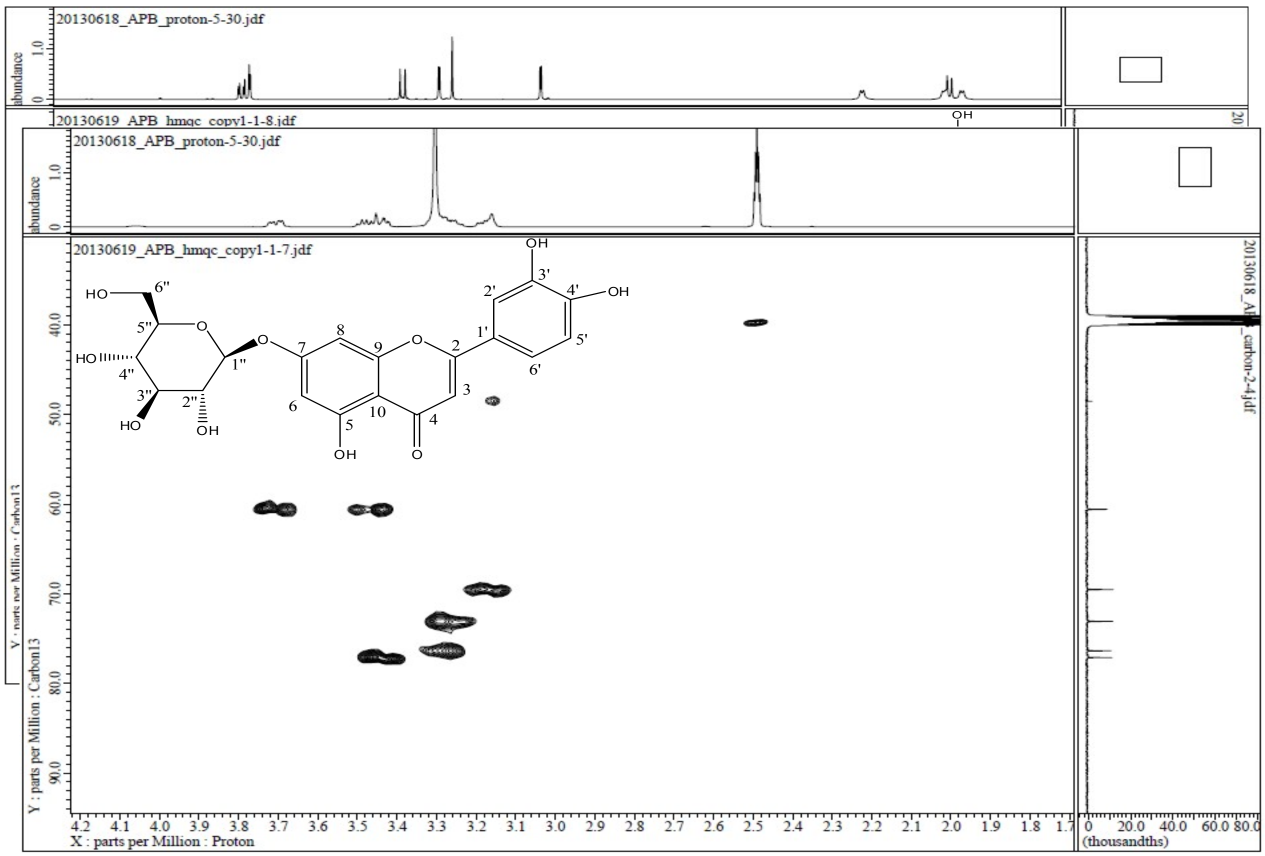

Fig. S4b. Expanded HMQC spectrum of luteolin-7-O-β-D-glucoside (**APB**) in DMSO-d_6.

Fig. S4c. Expanded HMQC spectrum of luteolin-7-O-β-D-glucoside (**APB**) in DMSO-d_6.

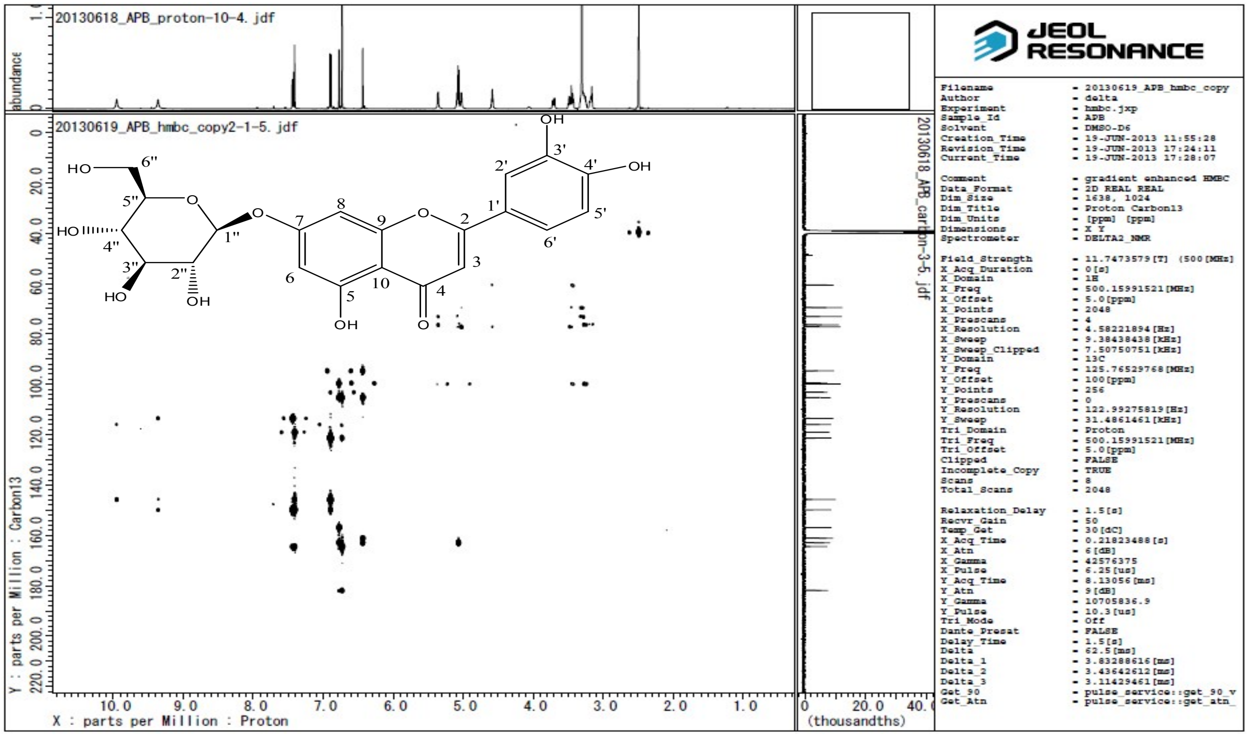

Fig. S5a. HMBC spectrum of luteolin-7-O-β-D-glucoside (**APB**) in DMSO-d_6.

Fig. S5b. Expanded HMBC spectrum of luteolin-7-O-β-D-glucoside (**APB**) in DMSO-d_6.

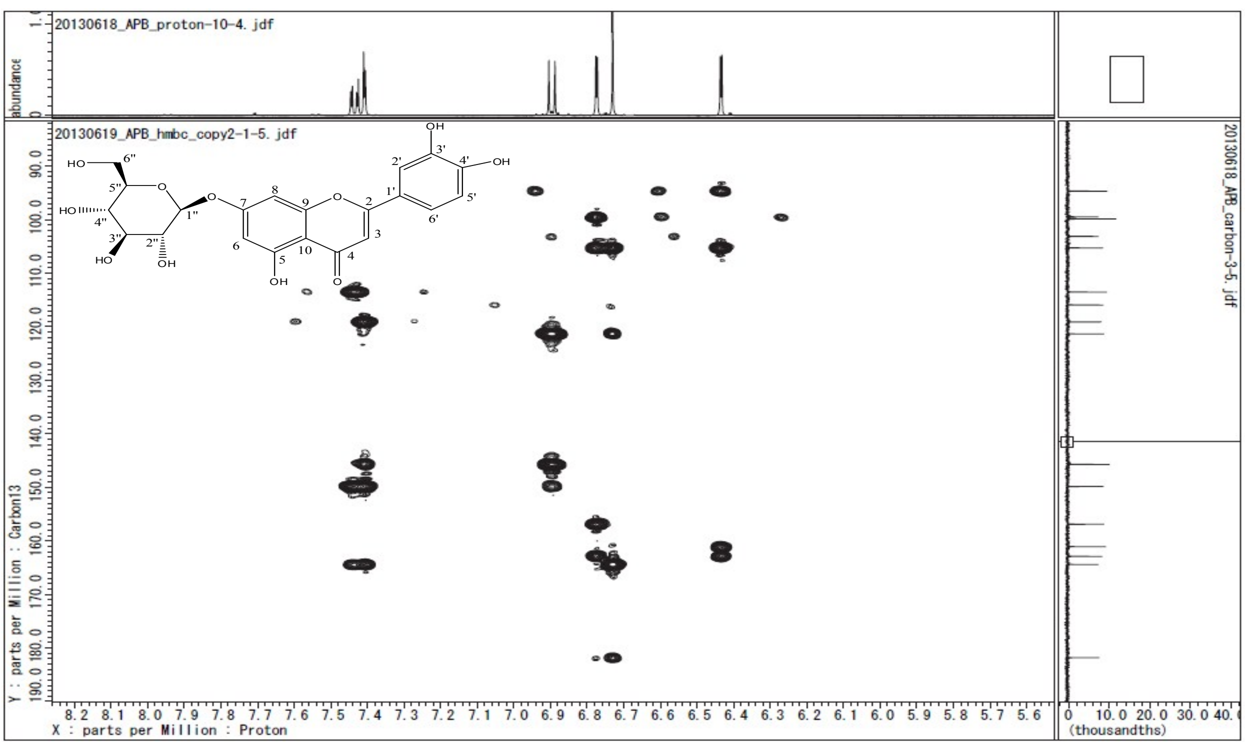

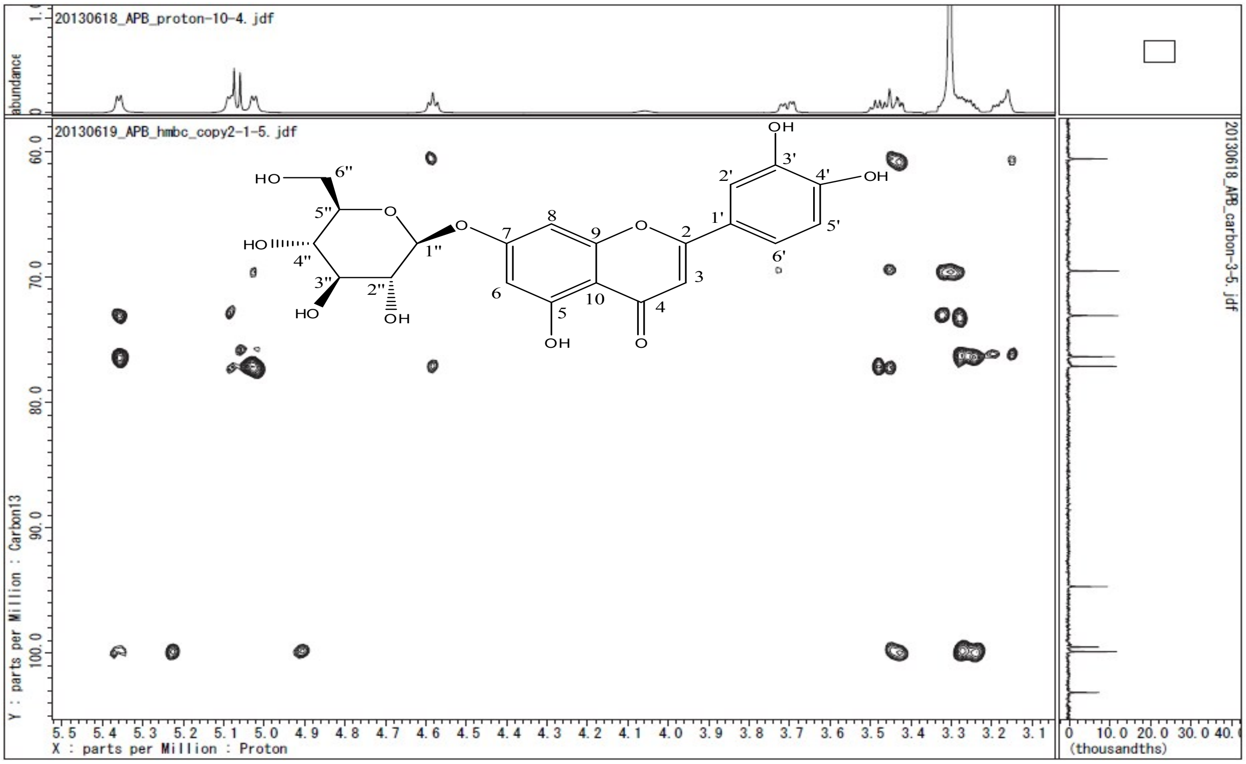

Fig. S5c. Expanded HMBC spectrum of luteolin-7-O-β-D-glucoside (**APB**) in DMSO-d_6.

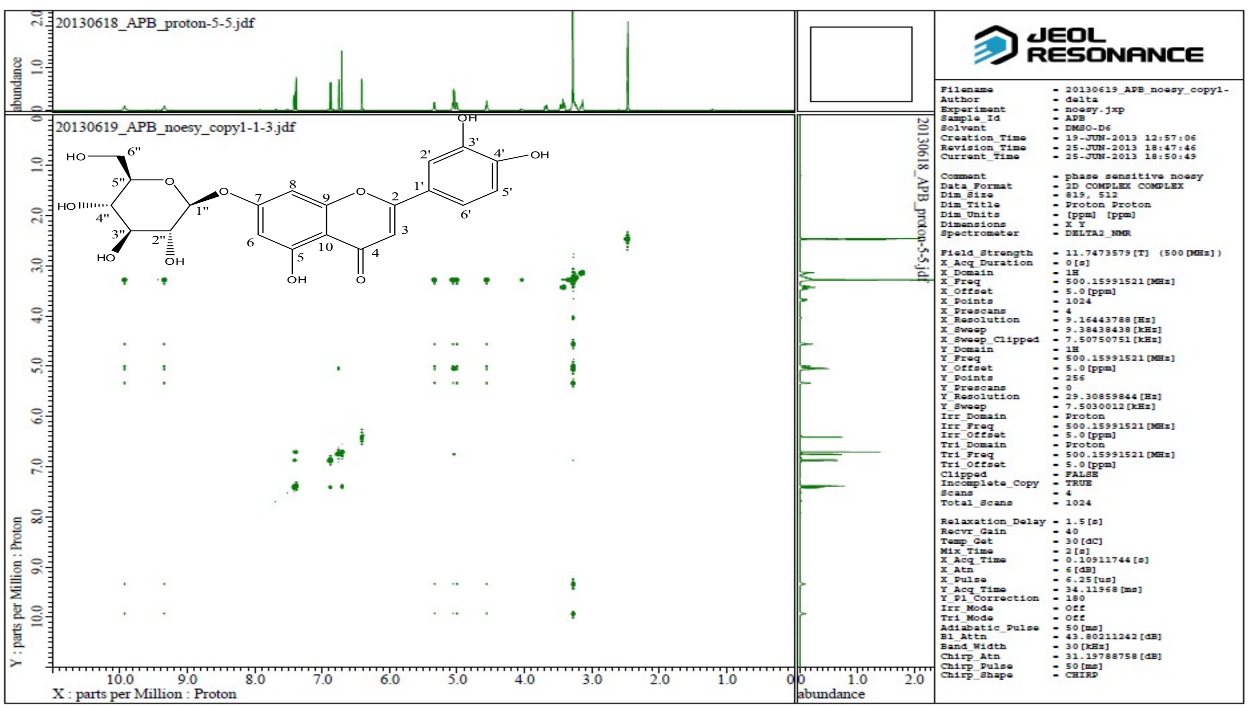

Fig. S6. NOESY spectrum of luteolin-7-O-β-D-glucoside (**APB**) in DMSO-d_6.

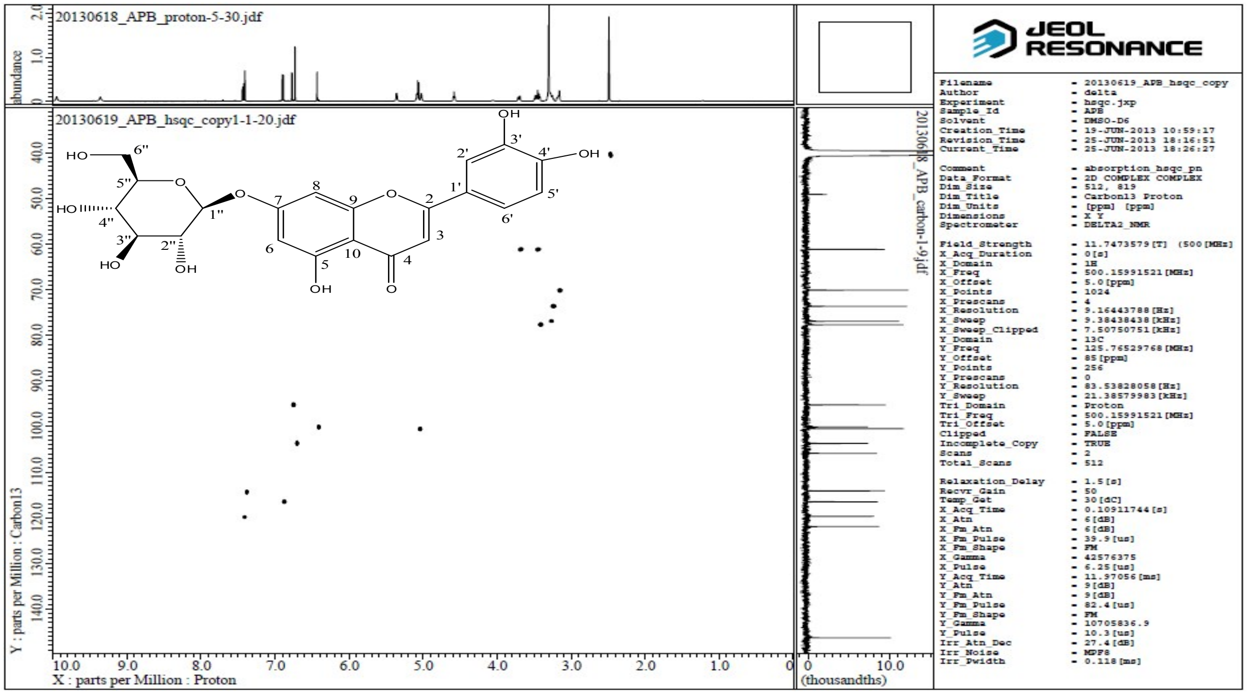

Fig. S7a. HSQC spectrum of luteolin-7-O-β-D-glucoside (**APB**) in DMSO-d_6.

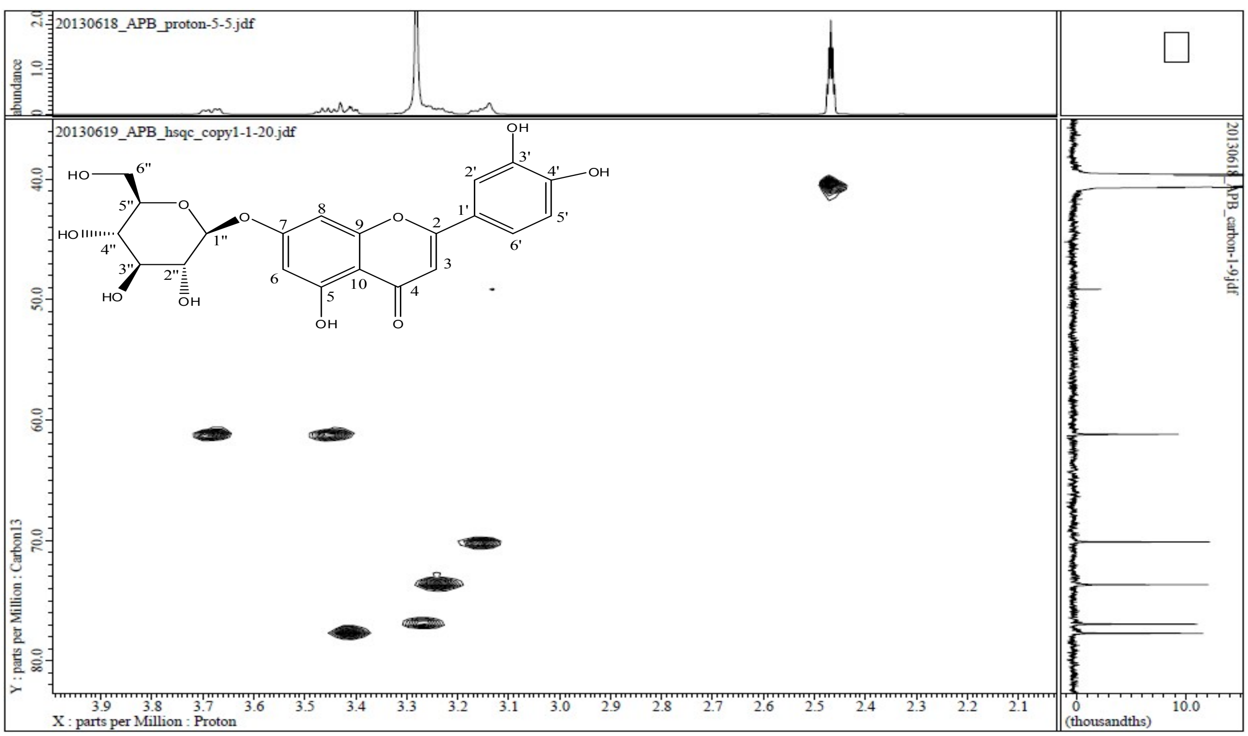

Fig. S7b. Expanded HSQC spectrum of luteolin-7-O-β-D-glucoside (**APB**) in DMSO-d_6.

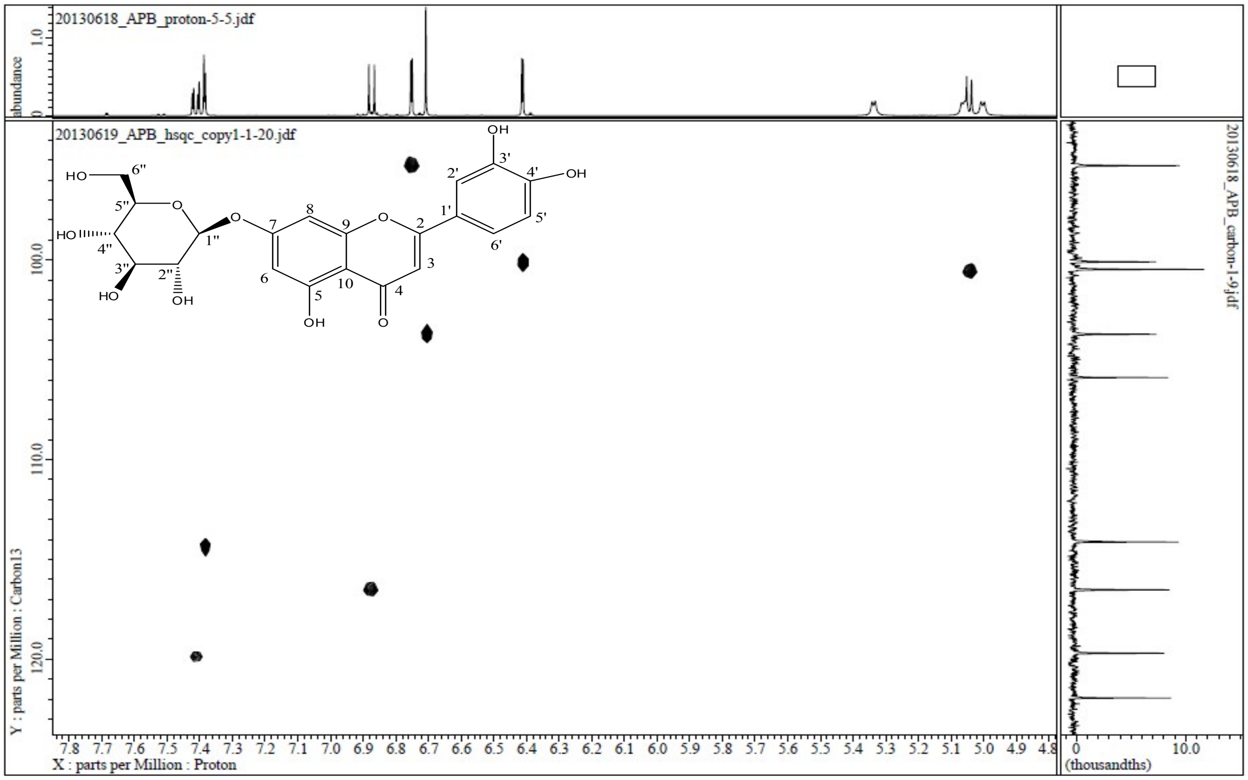

Fig. S7c. Expanded HSQC spectrum of luteolin-7-O-β-D-glucoside (**APB**) in DMSO-d_6.

Fig. S8. ESI-MS spectrum of luteolin-7-O-β-D-glucoside (**APB**) in negative ion mode.

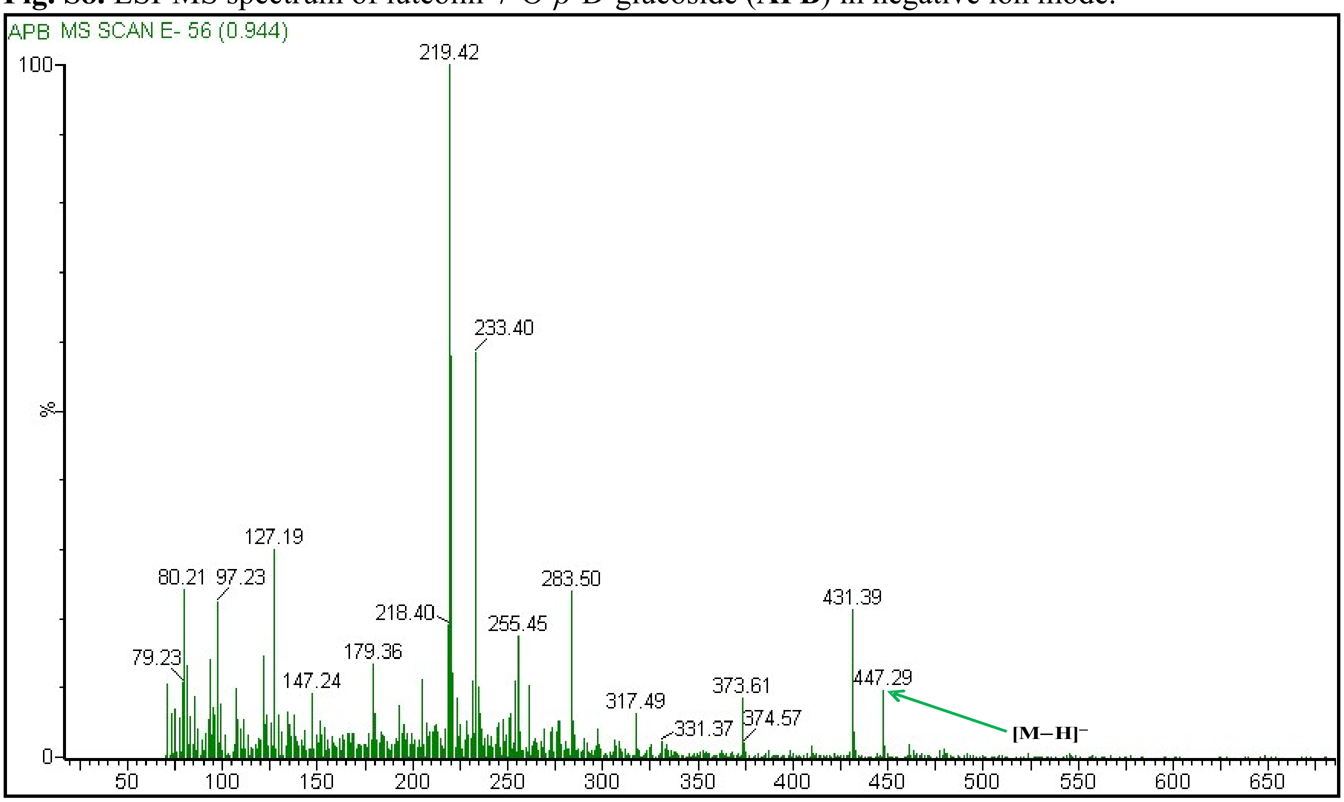

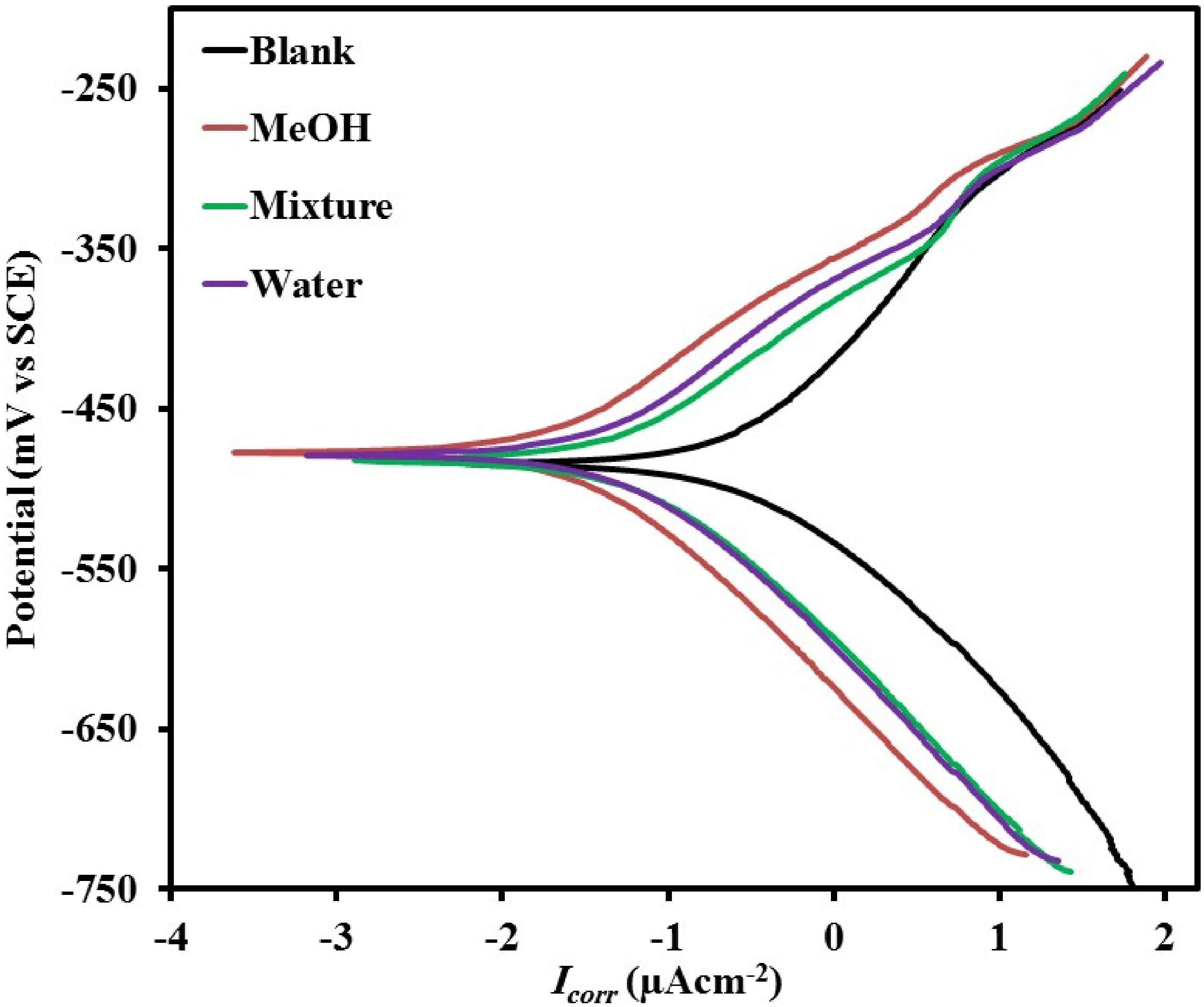

Fig. S9. Tafel plots in absence and presence of 600 ppm of MeOH, mixture and water extracts of *A. pseudocotula* in 1.0 M HCl.

Table-S1: Potentiodynamic polarization parameters obtained from Tafel plots for the corrosion of mild steel in 1.0 M HCl with 600 ppm of various extracts of *A. pseudocotula*.

Inhibitors	E_{corr} (mV)	I_{corr} (µAcm^{-2})	β_a (mV/dec)	β_c (mV/dec)	R_p	IE % Tafel	IE % LPR
Blank	−486.6	213.0	99.85	− 110.73	54.5	-	-
MeOH	−477.6	18.0	73.8	−64.6	446.8	91.6	87.8
Mixture MeOH: H_2O (85:15)	−482.7	50.0	75.0	−77.9	206.3	76.5	73.6
Water	−478.7	37.9	78.4	−72.7	250.3	82.2	78.2

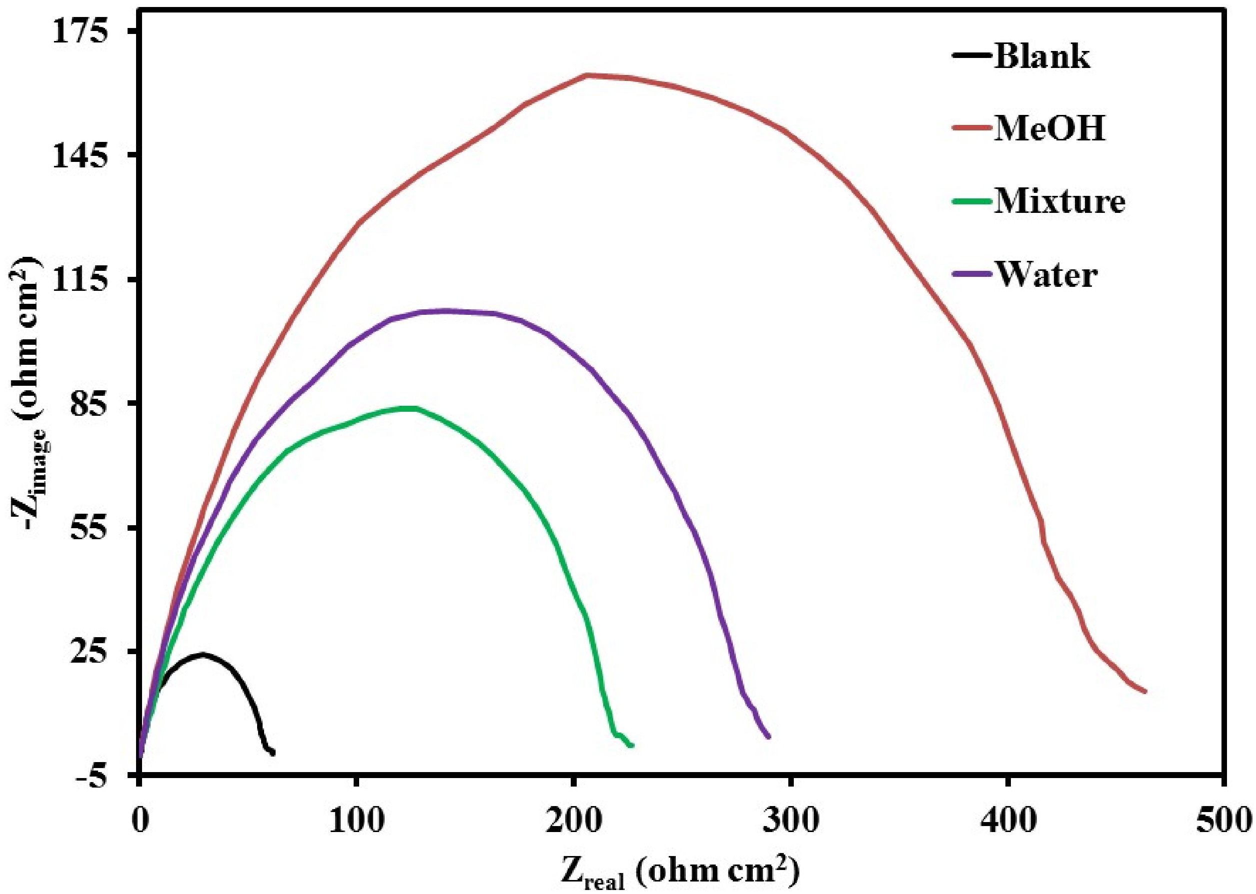

Fig. S10. Nyquist plots in absence and presence of 600 ppm of MeOH, mixture and water extracts of *A. pseudocotula* in 1.0 M HCl.

Table-S2: Electrochemical impedance parameters obtained from Nyquist plots for mild steel in 1.0 M HCl with 600 ppm of various extracts of *A. pseudocotula*.

Inhibitors	R_{ct} (Ω cm^2)	C_{dl} (μF cm^{-2})	θ	IE %
Blank	57.1	533.0	-	-
MeOH	445.3	145.0	0.87	87.2
Mixture MeOH: H_2O (85:15)	224.0	230.0	0.75	74.5
Water	274.0	250.0	0.79	79.2

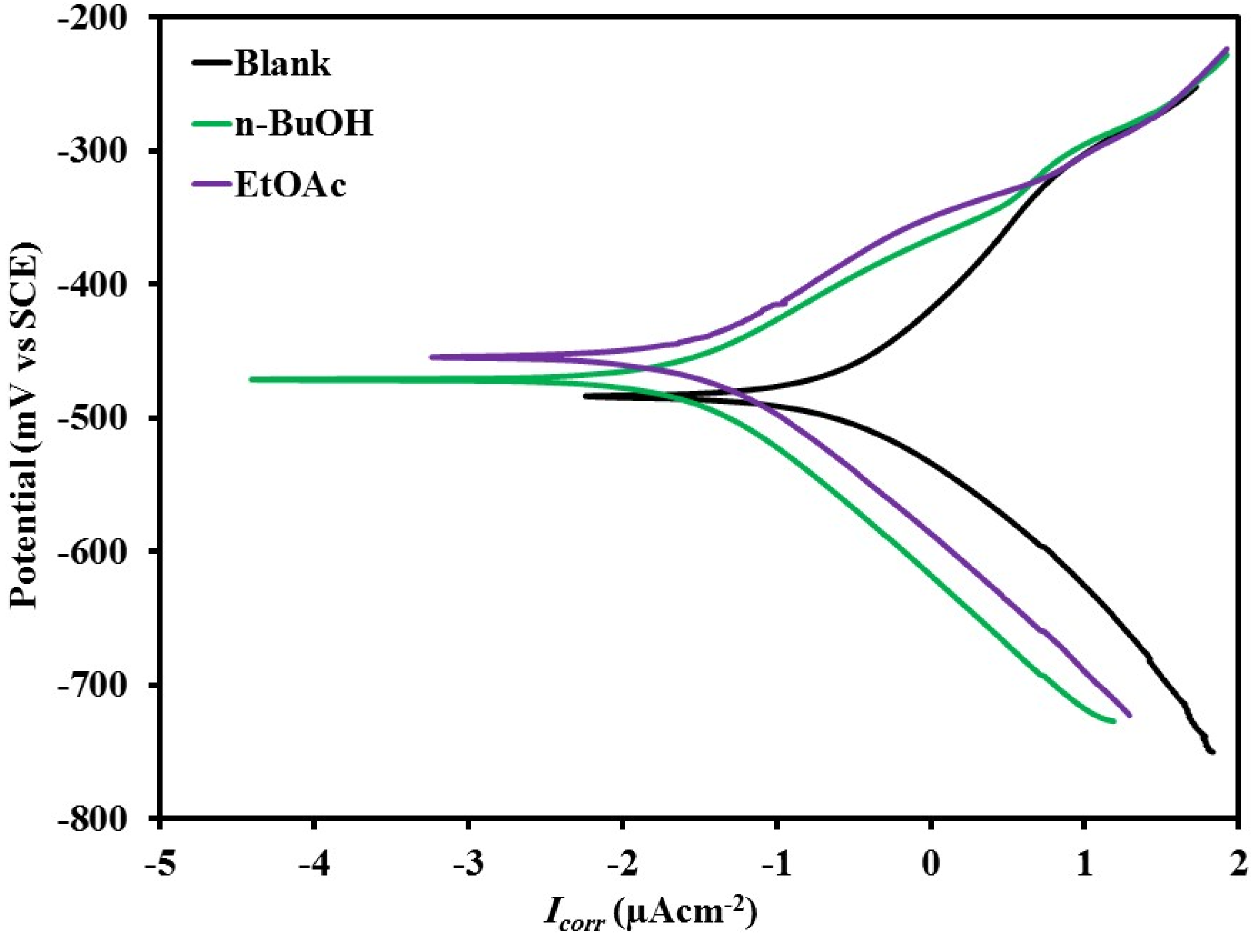

Blank
n-BuOH
EtOAc
-200
-300
-400
-500
-600
-700
-800
Potential (mV vs SCE)
-5
-4
-3
-2
-1
0
1
2
I_{corr} (µAcm^{-2})

Fig. S11. Tafel plots in absence and presence of *n*-BuOH and EtOAc extracts of *A. pseudocotula* in 1.0 M HCl.

Table-S3: Potentiodynamic polarization parameters obtained from Tafel plots for the corrosion of mild steel in 1.0 M HCl with 600 ppm of *A. pseudocotula* various extracts.

Inhibitors	E_{corr} (mV)	I_{corr} (μAcm^{-2})	β_a (mV/dec)	β_c (mV/dec)	R_p	IE % Tafel	IE % LPR
Blank	- 486.6	213.0	99.85	− 110.73	54.5	-	-
n-BuOH extract	- 472.3	21.9	69.3	- 74.84	399.1	89.7	86.3
EtOAc extract	- 454.9	33.2	78.0	- 86.25	303.8	84.4	82.1

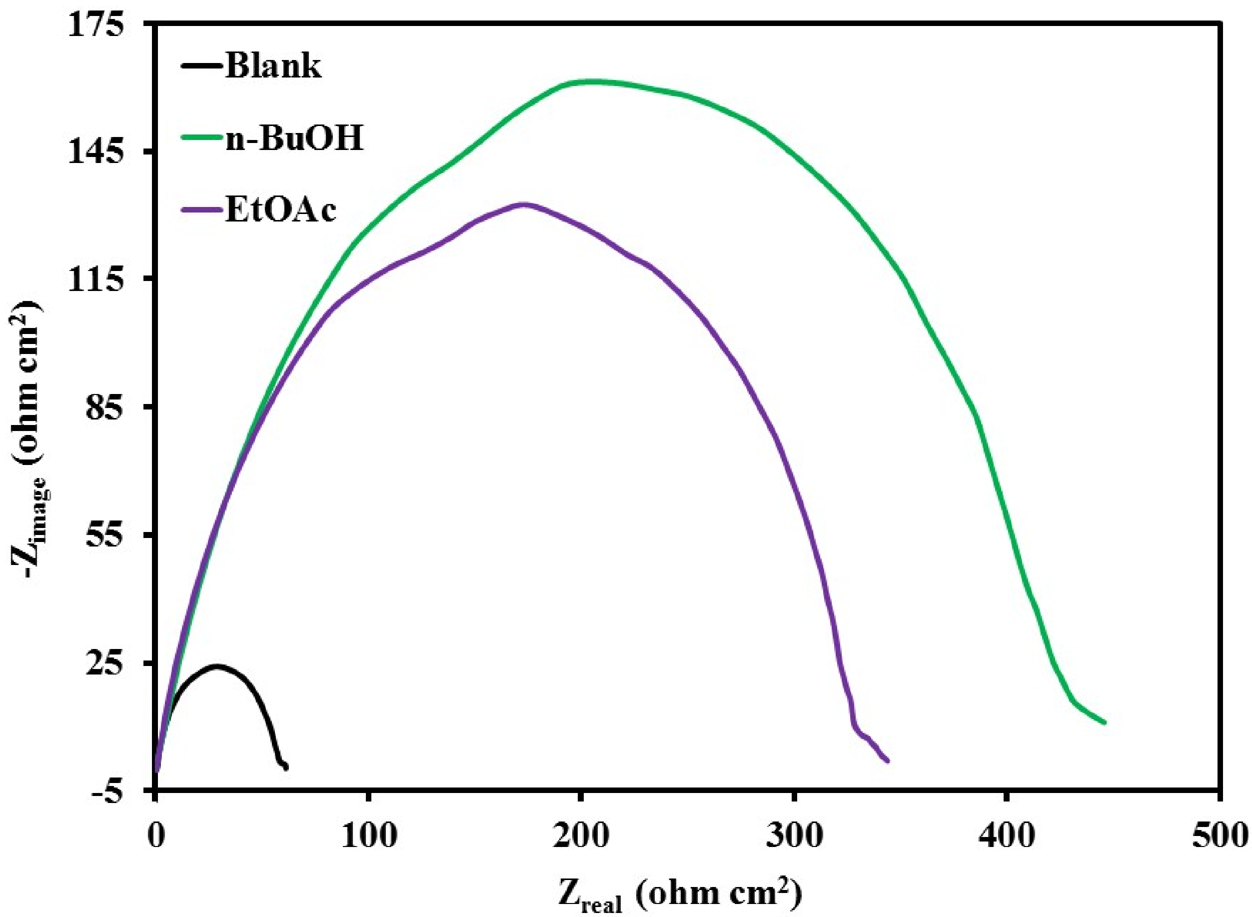

Fig. S12. Nyquist plots in absence and presence of *n*-BuOH and EtOAc extracts of *A. pseudocotula* in 1.0 M HCl.

Table-S4: Electrochemical impedance parameters obtained from Nyquist plots for mild steel in 1.0 M HCl with 600 ppm of *A. pseudocotula* various extracts.

Inhibitors	R_{ct} (Ω cm^2)	C_{dl} (μF cm^{-2})	θ	IE %
Blank	57.1	533.0	-	-
n-BuOH extract	428.5	149.0	0.87	86.7
EtOAc extract	331.4	142.0	0.83	82.8

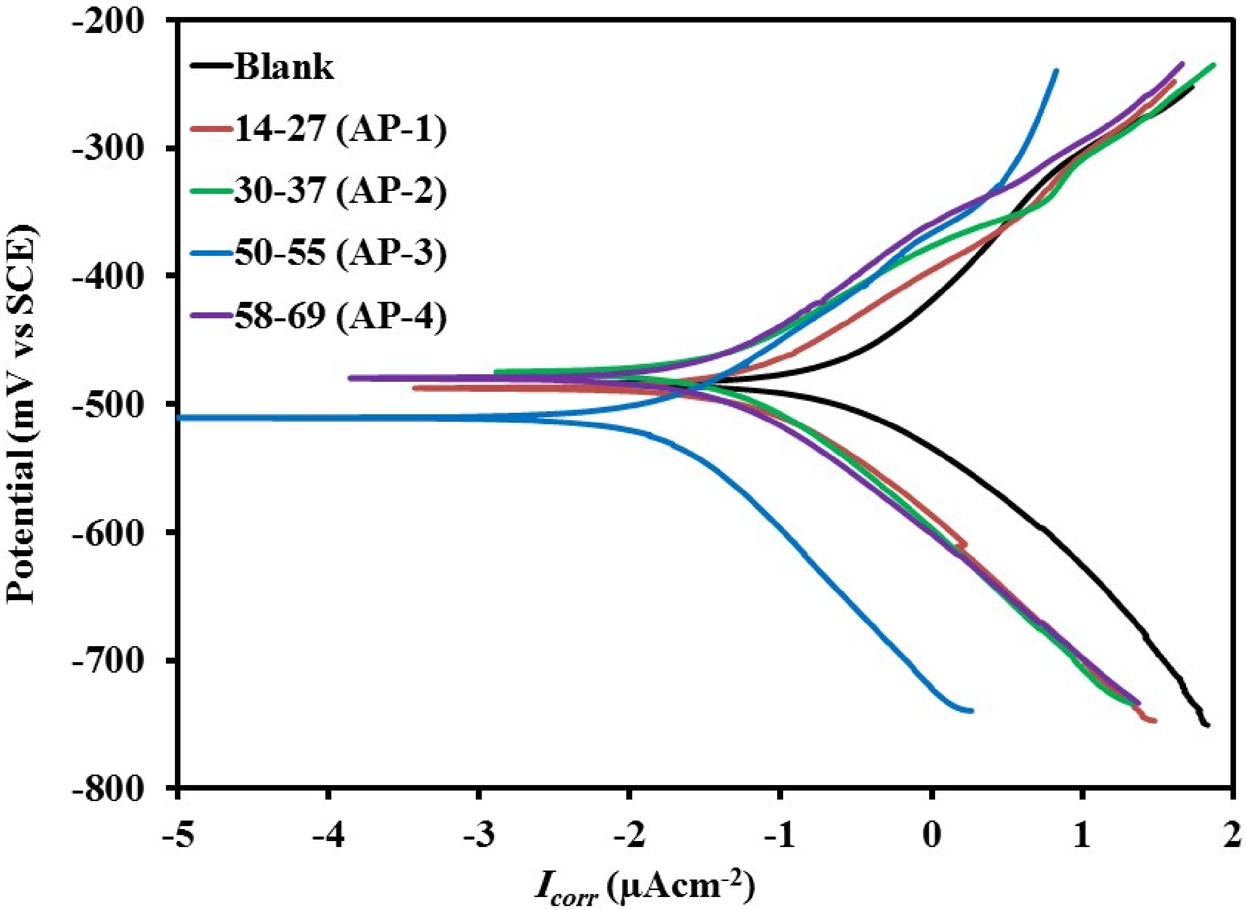

Blank
14-27 (AP-1)
30-37 (AP-2)
50-55 (AP-3)
58-69 (AP-4)
Potential (mV vs SCE)
-200
-300
-400
-500
-600
-700
-800
-5
-4
-3
-2
-1
0
1
2
Icorr (μAcm-2)

Fig. S13. Tafel plots in absence and presence of various fractions of *n*-BuOH extracts of *A. psuedocotula* in 1.0 M HCl.

Table-S5: Potentiodynamic polarization parameters obtained from Tafel plots for the corrosion of mild steel in 1.0 M HCl with 600 ppm of various fractions of *A. pseudocotula n*-BuOH extarcts.

Inhibitors	E_{corr} (mV)	I_{corr} (µAcm^{-2})	β_a (mV/dec)	β_c (mV/dec)	R_p	IE % Tafel	IE % LPR
Blank	- 486.6	213.0	99.85	− 110.73	54.5	-	-
AP-1	- 487.9	55.5	74.7	− 71.8	193.9	73.9	71.9
AP-2	− 476.3	47.8	81.8	− 86.9	210.9	77.6	74.2
AP-3*	− 510.1	11.7	53.1	− 66.0	1007.5	94.5	94.6
AP-4	− 479.3	38.2	86.2	- 84.1	279.3	82.1	80.5

* Tested with 200 ppm.

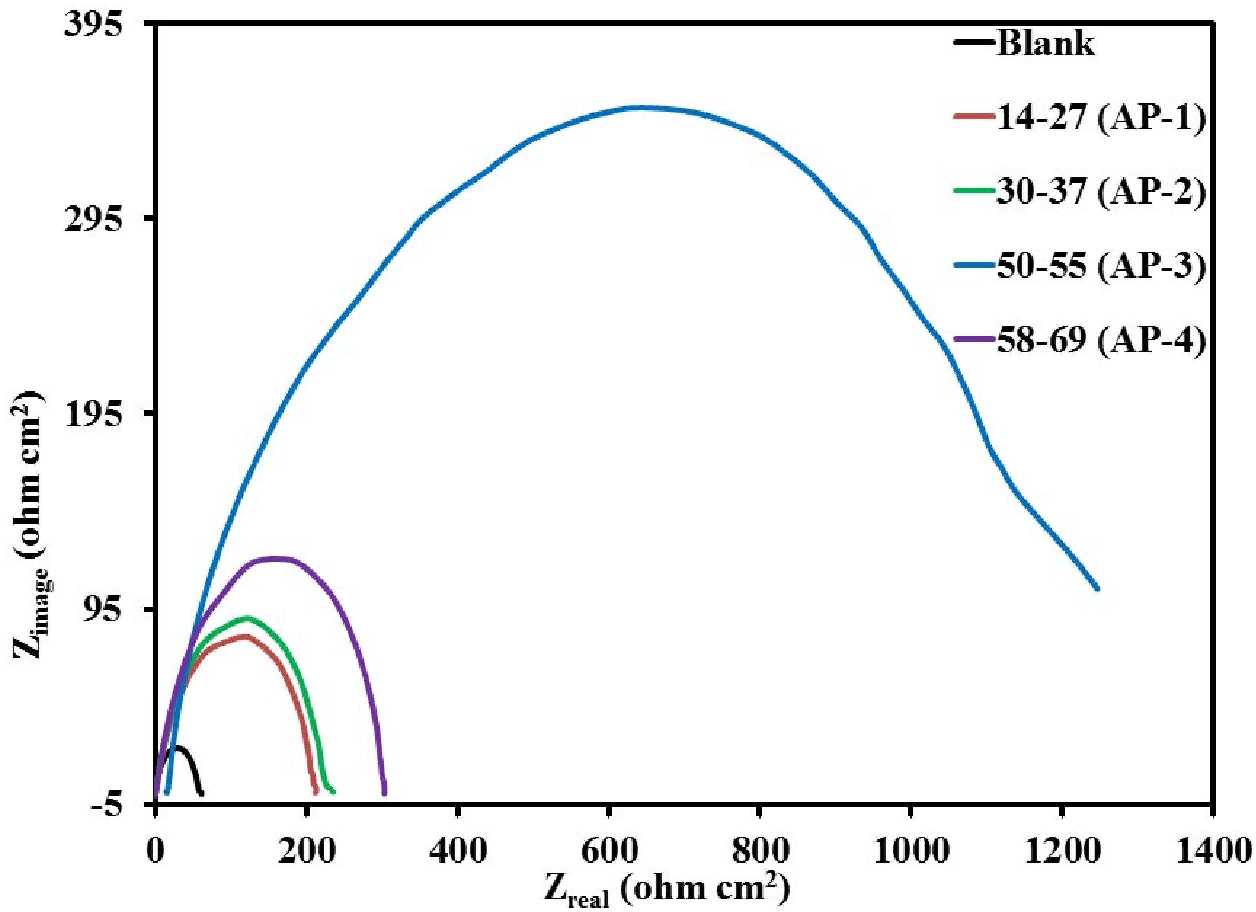

Fig. S14. Nyquist plots in absence and presence of various fractions of *n*-BuOH extracts of *A. psuedocotula* in 1.0 M HCl.

Table-S6: Electrochemical impedance parameters obtained from Nyquist plots for mild steel in 1.0 M HCl with 600 ppm of various fractions of *A. pseudocotula n*-BuOH extarcts.

Inhibitors	R_{ct} (Ω cm^2)	C_{dl} (μF cm^{-2})	θ	IE %
Blank	57.1	533.0	-	-
AP-1	217.6	226	0.74	73.8
AP-2	224.8	190	0.75	74.6
AP-3*	1040.0	175.0	0.95	94.5
AP-4	309.4	207	0.82	81.6

* Tested with 200 ppm.